Indian Academy of Sciences Conference Series (2020) 3:1
DOI: 10.29195/iascs.03.01.0006

Fractal structures in the deflection of light by a pair of Schwarzschild black holes

E. E. DE SOUZA FILHO[1], A. C. MATHIAS[1], I. L. CALDAS[2] and R. L. VIANA[1,*]

[1] Departamento de Física, Universidade Federal do Paraná, Curitiba, Paraná, Brazil
[2] Departamento de Física Aplicada, Instituto de Física da Universidade de São Paulo, São Paulo, São Paulo, Brazil
[*]Corresponding author. E-mail: viana@fisica.ufpr.br

Abstract. The deflection of light by the strong gravitational field produced by a pair of supermassive Schwarzschild black holes is considered from the point of view of an open conservative nonlinear dynamical system. From an approximate solution of the geodesic equation we obtained a two-dimensional map describing the impact parameter and scattering angle just before the light deflection by each black hole. Since the system is typically non-integrable, there is a parameter range for which chaotic area-filling orbits occur. The dynamics underlying those chaotic orbits involves a number of fractal structures related to the existence of a non-attractive invariant chaotic set. The outcome of a typical light ray approaching the system can be either diverged to infinity or falling into one of the black holes. Non-typical light rays can orbit around the black hole pair as periodic orbits. We identified the corresponding escape basins and their fractal boundaries, using two approaches: the computation of the uncertainty exponents and the corresponding basin and basin boundary entropies. We also exhibited the so-called Wada property showing qualitative pieces of evidence of this property.

Keywords. Black holes; fractal structures; fractal basins; Wada basins.

PACS Nos **05.45.-a; 05.45.Ac; 04.70.Bw**

1. Introduction

In general relativity we represent dynamics as geodesic motion in a curved space [1]. In this sense, if the curvature is negative there is sensitive dependence on initial conditions, which is a necessary condition for chaotic motion, although there are other conditions which must be verified like mixing of trajectories and compactness [2]. Fractal structures are quite common in chaotic systems, like chaotic attractors, basin boundaries, invariant manifolds, and so on [3]. In particular, open chaotic systems present a variety of fractal structures caused by the existence of an invariant non-attracting chaotic manifold, the so-called strange saddle [4].

One outstanding example is the chaotic scattering of particles, for which the presence of a strange saddle is responsible for a fractal distribution of scattered particles [5]. The presence of fractal structures in open non-integrable Hamiltonian systems with chaotic motion has been described in many situations of physical interest, like the motion of a star around a galactic centre [6, 7], open billiards [8, 9], drift motion of magnetically confined charged plasma particles [10], magnetic field lines in tokamaks [11], among others.

Supermassive cosmic objects, like black holes, generate space-time curvature, which leads to the deviations of the light rays, as they trace out null geodesics in the curved geometry [12]. Binary black holes rotate around their centre of mass and their existence has been confirmed by the observation of gravitational waves by LIGO Scientific Collaboration [13]. In such systems it is usually the case where the relative velocities are much smaller than c, and it is possible to approximate them as fixed in space.

The null geodesics equations describing the light ray scattering by a pair of black holes are non-integrable and constitute an open conservative dynamical system for which chaotic motion is possible [14]. One such example is the Majumdar–Papapetrou binary black hole, where a system of two charged black holes are in static equilibrium due to its electrostatic repulsion [15, 16]. The presence of fractal structures in this system, due to the chaoticity of geodesic motion, has been investigated by many researchers [17, 18].

The basic fractal structure to be investigated in a binary black hole system is the escape basin, which is the set of initial conditions leading to one of the three possible outcomes for a light ray when it encounters such a system: falling into the first or the second black hole or escaping to infinity. Such escape basins are very important in astrophysical investigations, since they are actually the so-called shadows of a black hole. A shadow is a region in the observer's sky which cannot be illuminated by distant light sources due to the blockage of a black hole [19]. Daza and coworkers have investigated escape basins in a Majumdar–Papapetrou binary black hole, showing that the escape basin boundaries are not only just fractal but also display the stronger Wada property: any boundary point belongs to the boundary of at least two other basins [14].

The investigation of fractal exit basins in the Majumdar–Papapetrou binary black hole system needs the numerical integration of the geodesic equations for a light ray in the form of a Hamiltonian system. An alternative approach was proposed by de Moura and Letelier and consists of obtaining a two-dimensional map describing the scattering of light rays by a system of two static Schwarzschild black holes [20]. The black holes are supposed so far apart from each other that the light ray motion in the neighbourhood of one black hole is not appreciably affected by the other black hole. In this way the action of each black hole on light rays can be studied separately using the exact solution for Schwarzschild black holes [21]. In Ref. [20] the fractality of the escape basin boundary was evidenced through numerical computation of the uncertainty dimension.

In this paper we continue the investigation opened by the scattering map derived in Ref. [20], through two lines of further development. Firstly we consider a general approach which enables us to describe each black hole using a spherically symmetrically metric, using an approximation for the scattering angle by each black hole and combining it with the second black hole to obtain a scattering map similar to that derived by de Moura and Letelier but with a different dependence of the scattering angle on the impact parameter [22]. The second contribution of our work is to characterise the fractality of the escape basin using not only the uncertainty method to compute the escape fractal basin boundary dimension, but also the recently developed notion of basin entropy, which is a measure of final-state uncertainty related to the fractality of the escape basin boundary [23]. Moreover we also include numerical evidence of the Wada property in the escape basins generated by the scattering map.

This paper is organised as follows: in the first section we outline the basic formulas for the scattering of a light ray by a spherically symmetric black hole. In section 2 we outline the approximate solution of the geodesics equation for the light ray deflection under the gravitational field of two Schwarzschild black holes. Section 3 is devoted to a description of the two-dimensional scattering map describing the light ray deflection due to the binary black hole system, also discussing some of its dynamical properties. Section 4 contains a description of the corresponding escape basins. Section 5 deals with the characterisation of escape basin using the uncertainty dimension, which is a measure of the fractality of such structures, as well as the basin entropy and basin boundary entropy related to them. The presence of the Wada property in the escape basins is examined in section 6. The last section contains our conclusions.

2. Basic equations

We use a four-dimensional space-time metric $g_{\mu\nu}$ with signature $(+,-,-,-)$, as well as Einstein's summation convention for repeated indexes. We use units where $c = G = 1$. In a curved space-time, light rays follow geodesics, whose equation is [1, 12]

$$g_{\mu\nu}dx^{\mu}dx^{\nu} = 0, \tag{1}$$

where we consider a metric for a symmetrically spherical and static space-time with length element

$$ds^2 = A(r)\,dt^2 - B(r)\,dr^2 - C(r)\left(d\theta^2 + \sin^2\,\theta\,d\phi^2\right), \tag{2}$$

where $A(r)$, $B(r)$ and $C(r)$ define the metric produced by the black hole.

Choosing $\theta = \pi/2$ for convenience, and introducing a parameter λ, the following general equation for the geodesics is obtained:

$$A(r)\left(\frac{dt}{d\lambda}\right)^2 - B(r)\left(\frac{dr}{d\lambda}\right)^2 - C(r)\left(\frac{d\phi}{d\lambda}\right)^2 = 0. \tag{3}$$

Both the energy E and angular momentum J are constants of motion, given by

$$E = A(r)\,\frac{dt}{d\lambda}, \tag{4}$$

$$J = C(r)\,\frac{d\phi}{d\lambda}, \tag{5}$$

such that (3) is rewritten in the form

$$A(r)\,B(r)\left(\frac{dr}{d\lambda}\right)^2 + V_{\rm eff}(r) = E^2, \tag{6}$$

where we define the effective potential

$$V_{\rm eff}(r) = \frac{A(r)\,B(r)}{[C(r)]^2}\,J^2. \tag{7}$$

The photosphere radius r_m is an extremum of the effective potential (i.e., $(dV_{\rm eff}/dr)_{r_m} = 0$).

If we consider a photon approaching the black hole from infinity with impact parameter b, the following equation for the geodesics is obtained:

$$\frac{A(r)\,B(r)}{[C(r)]^2}\left(\frac{dr}{d\phi}\right)^2 + \frac{1}{[U(r)]^2} = \frac{1}{b^2}, \tag{8}$$

where $[U(r)]^{-2} = A(r)/C(r)$. After approaching the black hole with a minimum distance r_0 the photon is deflected and emerges out in other direction. This distance is called the critical impact parameter and, from (8), it is given by

$$b_m = \sqrt{\frac{C(r_0)}{A(r_0)}} \equiv \sqrt{\frac{C_0}{A_0}}. \tag{9}$$

On substituting (9) back into (8) it turns out that the angle of deflection is

$$\alpha = I(r_0) - \pi, \tag{10}$$

where

$$I(r_0) = \int_{r_0}^{\infty} dr \sqrt{\frac{B(r)}{C(r)}}\left[\frac{A_0}{A(r)}\,\frac{C(r)}{C_0}\right]^{-1/2}. \tag{11}$$

In the limit of strong gravitational fields we can expand (11) so as to obtain [22]

$$\alpha(r_0) = -a\,\ln\left(\frac{r_0}{r_m}\right) + c + O(r_0 - r_m)$$
$$\alpha(b) = -\bar{a}\,\ln\left(\frac{b}{b_m} - 1\right) + \bar{c} + O(b - b_m), \tag{12}$$

where a, $\bar{a}$, c, and $\bar{c}$ depend on the functions A, B, and C, evaluated at the photosphere radius r_m. Similar to (9) we have $b_m = \sqrt{C(r_m)/A(r_m)}$.

The evaluation of the expansion coefficients must be done carefully since the integral (11) diverges at r_0. In order to do so, we rewrite (11) as [22]

$$I(r_0) = \int_0^1 dz f(z, r_0)\,R(z, r_0), \tag{13}$$

where we define auxiliary variables

$$y = A(r), \qquad y_0 = A_0, \qquad z = \frac{y - y_0}{1 - y_0}, \tag{14}$$

and the following functions

$$R(z, r_0) = \frac{2\sqrt{B\,y\,C_0}}{C\,A'}(1 - y_0), \tag{15}$$

$$f(z, r_0) = \left\{y_0 - [(1 - y_0)z + y_0]\,\frac{C_0}{C}\right\}^{-1/2}. \tag{16}$$

We remark that $R(z, r_0)$ is regular for all values of z and r_0, whereas $f(z, r_0)$ diverges for $z \to 0$. Expanding the integrand of (16) up to second order terms we have

$$f(z, r_0) \approx f_0(z, r_0) = \sqrt{\frac{1}{\gamma\,z + \beta\,z^2}}, \tag{17}$$

where

$$\gamma = \frac{1 - y_0}{C_0\,A'_0}(C'_0 y_0 - C_0 A'_0), \tag{18}$$

$$\beta = \frac{(1 - y_0)}{2C_0^2 A'^3_0}\Big[2C_0 C'_0 A'^2_0 + \left(C_0\,C'_0 - 2\,C'^2_0\right) - C_0\,C'_0\,y_0\,A''_0\Big], \tag{19}$$

and the primes denote differentiation with respect to the argument.

Proceeding in this way we obtain the desired coefficients of the expansions in (12), as follows:

$$\bar{a} = \frac{a}{2} = \frac{R(0, r_m)}{2\sqrt{\beta_m}}, \tag{20}$$

$$\bar{c} = -\pi + c_r + \bar{a}\,\ln\left(\frac{2\,\beta_m}{y_m}\right), \tag{21}$$

where $\beta_m = \beta(r_m)$ and c_r is the real part of the integral (13).

In this paper we shall consider Schwarzschild black holes with mass M, such that these functions are given by the following expressions [21]:

$$A(r) = 1 - \frac{2\,M}{r}, \tag{22}$$

$$B(r) = \left(1 - \frac{2\,M}{r}\right)^{-1} = \frac{1}{A(r)}, \tag{23}$$

$$C(r) = r^2. \tag{24}$$

Schwarzschild black holes have one event horizon, given by the radius where the metric diverges, corresponding to $r = 2M$. Without loss of generality we may set $2M = 1$. For the Schwarzschild metric the coefficients (18) and (19) are given, respectively, by

$$\alpha = 2 - \frac{3}{r_0}, \tag{25}$$

$$\beta = \frac{3}{r_0} - 1. \tag{26}$$

Using (22)–(24) in (7) and computing the extremum of the effective potential results that the radius of the photosphere is $r_m = 3/2$, in such a way that (19) gives $\beta_m = 1$. From these results, the coefficients (20) and (21) of the expansion for the deflection angle (12) are

given by

$$\bar{a} = 1, \tag{27}$$

$$\bar{c} = -\pi + b_m + \ln 6 \approx -0.4002, \tag{28}$$

$$b_m = \frac{3\sqrt{3}}{2} \approx 2.5981, \tag{29}$$

$$c_r = 2 \ln[6(2 - \sqrt{3})] \approx 0.9496. \tag{30}$$

The scattering of a light ray by a single black hole can now be understood in terms of the possible values of the corresponding impact parameter b. A light ray comes from infinity and approaches the black hole with impact parameter b and whose direction makes a deflection angle α given by (10). If $b < b_m \approx 2.5981$ the light ray falls into the black hole and disappears. On the other hand, for this light ray not to escape back to infinity it is necessary that its impact parameter b be such that the deflection angle α be at least π. Hence we additionally have $b < b_{\rm esc}$, where $\alpha(b_{\rm esc}) = \pi$. Using (12), (27), and (28) this means that

$$b_{\rm esc} = b_m \left[\exp\left(\frac{\bar{c} - \pi}{\bar{a}} \right) + 1 \right] \approx 2.67332. \tag{31}$$

As a result, for a light ray deflected by a single black hole not to escape to infinity or to collide with a black hole, the impact parameter must belong to the narrow interval $b_m < b < b_{\rm esc}$.

3. The scattering map

After deriving the equations for the deflection of a light ray by a single black hole, we now consider a system of two identical black holes separated by a distance D with the same mass $M = 1/2$ (figure 1). Such binary systems rotate around their centre of mass [24] and their existence has been confirmed by the observation of gravitational waves from a binary black hole merging by LIGO Scientific Collaboration [13]. In such systems it is usually the case where the relative velocities are much smaller than c, and it is possible to approximate them as fixed in space.

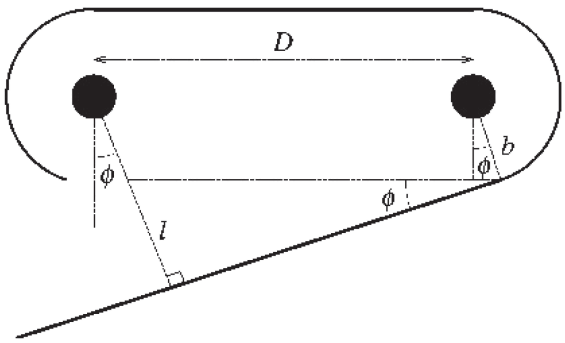

Figure 1. Schematic figure showing the basic geometrical elements involved in the scattering map for the light ray deflection by a pair of black holes.

Unlike the case of a single black hole treated in the previous section, such a system has no exact solution of field equations. In spite of this, if the distance D between the black holes is much higher than their Schwarzschild radius ($r_0 = 2M = 1$) then the nonlinear interaction between their gravitational fields can be neglected. In this case we consider the deflection of light from each black hole in a separate way using the expressions previously found for the Schwarzschild metric. In other words, in the light scattering by a given black hole the effect of another black hole is neglected. Both approximations are discussed in detail in Ref. [20]. In particular, these approximations may not hold if we consider the scattering of massive test particles.

The line connecting the two black holes will be the axial symmetry axis. We shall assume that light rays have zero angular momentum in this direction. As a result, the light rays are constrained to move in the plane containing the two black holes [24]. The basic geometry involved in the light scattering by the binary black hole is depicted in figure 1: a light ray comes from infinity and approaches the first black hole with impact parameter b and whose direction makes an angle ϕ with the axial symmetry line.

For this light ray not to escape back to infinity it is necessary that $b < b_{\rm esc}$, where $b_{\rm esc}$ is given by (31). Conversely, for the light ray not to fall to the first black hole the impact parameter must satisfy $b > b_m$. If the light ray is not deflected to infinity by the first black hole, then it goes to the other black hole and is deflected again. If not deflected to infinity it returns to the vicinity of the first black hole, and so on.

Instead of considering the detailed trajectories of the null geodesics corresponding to the light rays, it is often more convenient to define discretized variables (b_n, ϕ_n), corresponding respectively to the values of the impact parameter and angle with respect to the axial symmetry line in the neighbourhood of the nth scattering. Even (odd) values of n correspond to the first (second) black hole. Using such discrete time intervals the differential equations for light scattering reduce to a two-dimensional discrete-time map [20]

$$b_{n+1} = b_n + D\,\phi_n, \tag{32}$$

$$\phi_{n+1} = \pi + \phi_n - \alpha(b_{n+1}), \quad (\mathrm{mod}\, 2\pi) \tag{33}$$

where $\alpha(b)$ is given by (12). Some sign conventions are essential in this description: positive values of b imply that the light ray goes from black hole 1 to 2 (from 'left' to 'right' in figure 1), and negative values otherwise; whereas positive values of ϕ correspond to

counterclockwise rotations. In Ref. [20] this map was obtained from a different function $\alpha(b)$ resulted from the exact solution of Schwarzschild metric [21]. Our choice for $\alpha(b)$, on the other hand, resulted from a different procedure, which can be applied to *any* spherically symmetric and static black hole [22].

The Jacobian matrix of the scattering map (32) and (33) is

$$\mathbf{J} = \begin{pmatrix} 1 & D\,\cos\,\phi_n \\ -\alpha'(b_{n+1}) & 1 - D\,\alpha'(b_{n+1})\,\cos\,\phi_n \end{pmatrix} \tag{34}$$

whose determinant is equal to unity, such that the scattering map (32) and (33) is an area-preserving mapping, corresponding to the following continuous-time Hamiltonian:

$$H(b,\phi,n) = \pi\, b - \int^{b} db'\alpha(b') + D\,\delta_1(n)\cos\,\phi, \tag{35}$$

where

$$\delta_1(n) = \sum_{m=-\infty}^{\infty} \delta(n-m) = 1 + 2\sum_{q=1}^{\infty}\cos(2\pi q n), \tag{36}$$

is a periodic delta function (Dirac comb).

The fixed points of the scattering map are $\phi^*_{1,2} = 0, \pi$ and $b^*_{1,2} = b_{\rm esc}$. The eigenvalues of the Jacobian matrix (34) at these points are

$$\lambda_{1,2} = \frac{\tau}{2} \pm i\sqrt{1 - \left(\frac{\tau}{2}\right)^2}, \tag{37}$$

where

$$\tau = 2 - D\,\alpha'(b_{n+1})\cos\,\phi_n \tag{38}$$

is the trace of Jacobian matrix. These fixed points are stable provided $|\tau| < 2$. It turns out that the point $(b_{\rm esc}, 0)$ is stable if $0 < D\,\alpha'(b_{\rm esc}) < 4$, whereas the other fixed point $(b_{\rm esc}, \pi)$ is stable if $-4 < D\,\alpha'(b_{\rm esc}) < 0$. In either case the light ray trajectory is such that $b_{n+1} = -b_n$. Since $\alpha'(b_{\rm esc}) < 0$ and $D > 0$ the fixed point at $\phi = 0$ is always unstable (a hyperbolic saddle). If, in addition, we have $|\alpha'(b_{\rm esc})| > (4/D)$ the other fixed point at $\phi = \pi$ is also unstable.

For $D \neq 0$ the Hamiltonian (35) is generally non-integrable. On the other hand, by physical grounds, if the light deflection by one black hole must be independent of the existence of the other black hole, then we must assume that D is typically a large number. In such case both fixed points are unstable and we expect a sizeable area-filling chaotic orbit in the phase space (b, ϕ).

4. Escape basins

The deflection of light by a system of binary black holes is an example of open dynamical system, i.e., a system for which trajectories (light rays) eventually escape from a given phase space region. If there are more than one way by which trajectories can escape, then it is relevant to identify the sets of initial conditions that generate trajectories escaping through a given exit. This set is called the escape basin corresponding to that exit [5]. In the case of two or more exits we may identify the boundary which separates those escape basins, called escape basin boundary. It has been long known that conservative dynamical systems presenting chaotic dynamics have fractal escape basins and fractal escape basin boundaries [3].

In order to plot the escape basins corresponding to the scattering map (32) and (33), we choose a set of initial conditions (b_0, ϕ_0) and iterate them to find out to which basin they belong. We divide the phase space region $\Omega = \{0 \leq \phi_0 \leq 2\pi, b_m < b_0 < b_{\rm esc}\}$ in a large number of points and iterate the map (32) and (33) for each of these initial conditions, recording the final outcome for each point. Depending on its initial conditions, after a number of map iterations, a light ray may fall into one black hole (**A**), into the other black hole (**B**), or escapes towards infinity (**C**). All outcomes can be considered as exits since we stop iterating the map once a light ray falls into a black hole. Accordingly, we denote the corresponding escape basins to be $\mathcal{B}(\mathbf{A})$, $\mathcal{B}(\mathbf{B})$ and $\mathcal{B}(\mathbf{C})$.

Figure 2 is a representative example of the escape basins for the scattering map (32) and (33) when $D = 15$, which is a value large enough to ensure that each black hole deflects light rays in an independent fashion. We used a grid of $10^4 \times 10^4$ initial conditions over the phase space region Ω and iterate each initial condition

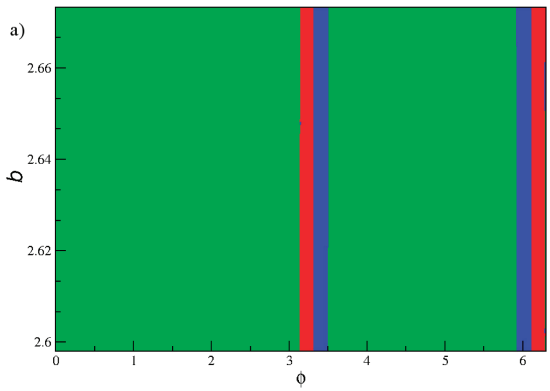

Figure 2. Escape basins for the scattering map when $D = 15$. Green points represent initial conditions generating orbits that escape to infinity. Red and blue points are the escape basins for black holes **A** and **B**, respectively.

by a maximum of 10^4 times. An orbit falls into a black hole whenever $b_n < b_m \approx 2.5981$ for a given escape time $n = \bar{n} < 10^4$. If $\bar{n}$ is even (odd) we know that the light ray falls into black hole **A** (**B**) and the corresponding initial condition is painted red (blue). If the orbit goes to infinity ($b_n > b_{\rm esc} \approx 2.67332$) for a given $n = \bar{n} < 10^4$ the corresponding initial condition is painted green. The red, blue, and green regions are thus numerical approximation for the exit basins $\mathcal{B}$(**A**), $\mathcal{B}$(**B**) and $\mathcal{B}$(**C**), respectively. There is a measure zero set of unstable periodic orbits which never escape and, since $D < \infty$, we cannot rule out orbits within very tiny periodic islands which do not escape at all, but whose effect in the exit basins would be negligible.

Since the labelling of black holes **A** and **B** is immaterial, their escape basins would be symmetric, i.e. they must have the same size. On the other hand, figure 2 shows that the dominant basin is that of infinity (**C**). The sequence of red and blue regions, however, has a fine structure that cannot be seen in figure 2, but requires further magnifications. This characterisation is also possible by defining a function $g(b)$ such that [20] $g(b) = 1$, if the orbit falls into black hole **A**, $g(b) = -1$, if it falls into **B**, and $g(b) = 0$ if the orbit escapes to infinity.

In order to investigate the escape basin boundary for the regions in figure 2 we analyse two regions in the vicinity of the points with $\phi_0 = 0$ and $\phi_0 = \pi$. For both regions, we divide the impact parameter interval $b_m < b < b_{\rm esc}$ into 10^6 points. The corresponding escape basins are plotted in (a) and (d), respectively, as a horizontal bar with green, red and blue stripes. We also plotted the corresponding function $g(b)$ below the bars. In figures 3b and e we show magnifications of two intervals of figures 3a and d, respectively, and figures 3c and f are further magnifications. These zoomings clearly show that there are regions for which there are pieces of the three escape basins in all scales. This self-similarity is a signature of the fractality of the basins as well as of its basin boundary.

Since some regions of different escape basins are intertwined in arbitrarily fine scales it is extremely difficult, if not impossible at all, to predict the final outcome of a light ray, given its initial condition being always

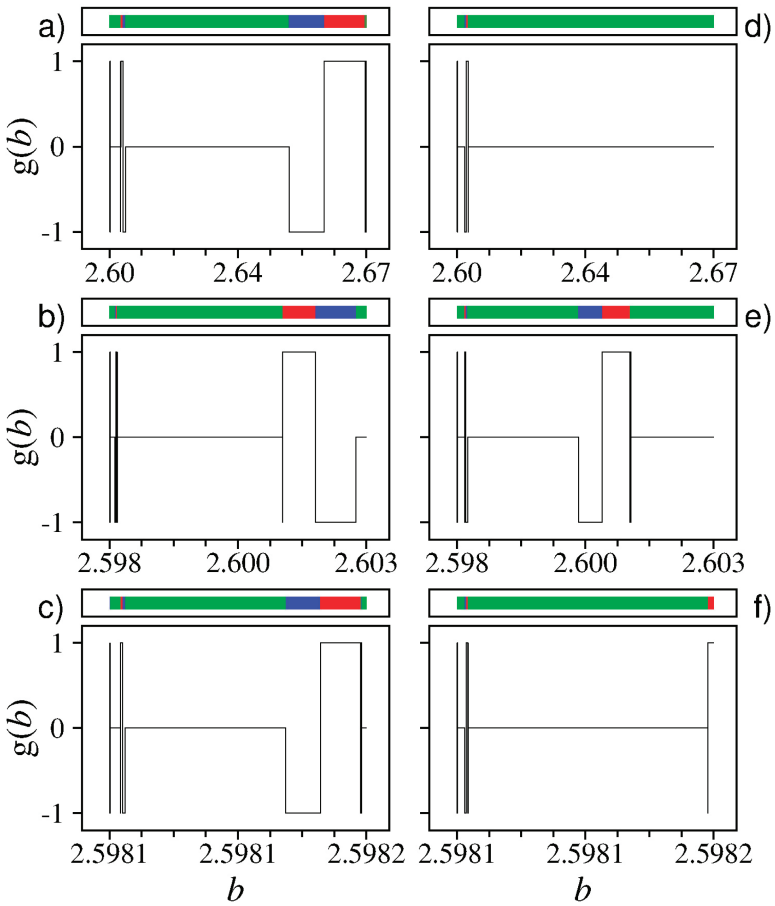

Figure 3. The horizontal bars represent the escape basins as a function of the impact parameter b for $\phi_0 = 0$ in (**a**), with magnifications in (**b**) and (**c**); and $\phi_0 = \pi$ in (**d**), with magnifications in (**e**) and (**f**). The colour code is the same as in figure 2. We plot, below the horizontal bars, the corresponding values of the function $g(b)$ (see text for details).

known up to a given uncertainty. One of the observable consequences of the existence of fractal structures in phase space is final-state sensitivity, i.e. small uncertainties in the initial conditions may lead to large uncertainties with respect to the future behaviour of the system [25].

The nature of the complicated structure of the escape basins displayed in figure 3 can be understood by considering the invariant chaotic set underlying the chaotic region in phase space. Let P be an unstable periodic point of the map embedded in the chaotic region, with its stable and unstable manifolds. The unstable and stable manifolds are sets of points which asymptote to the periodic orbit under forward and backward iterations of the map, respectively. The intersection of the stable and unstable manifolds of an infinite number of unstable periodic orbits, called a chaotic saddle, is a non-attracting invariant chaotic set with a dense chaotic orbit [4]. Initial conditions belonging to this chaotic saddle remain in the chaotic region, unless portions of the saddle cross the escape regions [26].

In order to get the invariant manifolds of the chaotic saddle we used the sprinkler method, which starts by partitioning the phase space region into a fine mesh of points. For each initial condition point we compute the escape time, i.e. the number of map iterations it takes for the corresponding orbit to leave the phase space region [27]. The stable manifold is formed by initial conditions set with a connection length larger than some specified value n_c, and the unstable manifold are their last iterations before leaving the phase space region [28]. The chaotic saddles are those initial conditions with a given connection length $\bar{n} = \xi n_c$, where $0 < \xi < 1$. To get the manifolds the values of n_c and ξ must be chosen after trial and error, but the numerical results seem not to be substantially affected by them [27].

Figure 4c shows a numerical approximation of the chaotic saddle resulting from the intersection of the stable and unstable manifolds illustrated in figures 4a and b, respectively. Starting from a grid of $10^3 \times 10^3$ initial conditions, we record those initial conditions with an escape time larger than $n_c = 40$. Such initial conditions constitute an approximation to the stable manifold of the chaotic saddle (figure 4a). On the other hand, the end points of the trajectories related to the recorded initial conditions (i.e., the orbit points for those trajectories after $n_c = 40$ map iterations), are an approximation to the unstable manifold of the saddle (figure 4b). The points from the middle of these trajectories ($\bar{n} = 0.5n_c = 20$) are thus representations for the chaotic saddle (figure 4c).

The connection between escape basin boundary and invariant manifold structure is similar to that exist for basins of attraction, and it is based on the fact that the

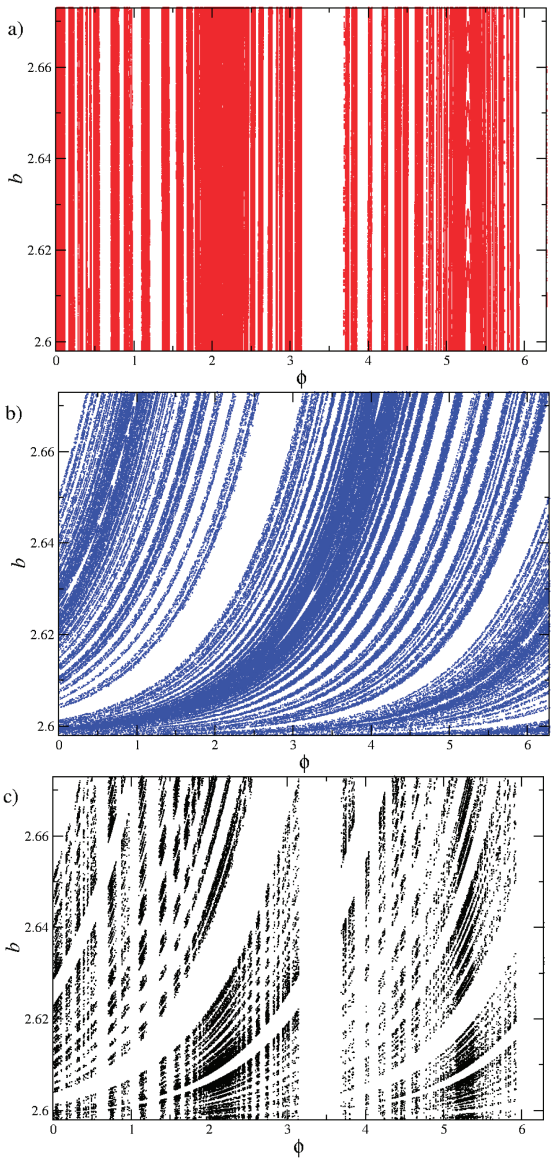

Figure 4. (**a**) Stable and (**b**) unstable manifold and (**c**) chaotic saddle for a chaotic orbit in the case of the scattering map for $D = 15$. The sprinkler method is used with $n_c = 40$ iterations and $\xi = 0.5$.

basin boundary is the closure of the stable manifold of a saddle periodic orbit P belonging to the chaotic saddle, under the map $\mathbf{F}$ (in our case, the scattering map (32) and (33)) [25]. We show this situation schematically in figure 5: let S to be a segment of the escape basin boundary to intercept the unstable manifold of P. The backward images of this segment, like $\mathbf{F}^{-1}(S)$ and $\mathbf{F}^{-2}(S)$ (figure 5) are smoothly deformed, becoming also increasingly elongated and accumulate at the stable manifold of P. This occurs because the intersections between the unstable manifold and the basin boundary converge exponentially fast according to the corresponding eigenvalue of the tangent map $\mathbf{DF}(P)$; and

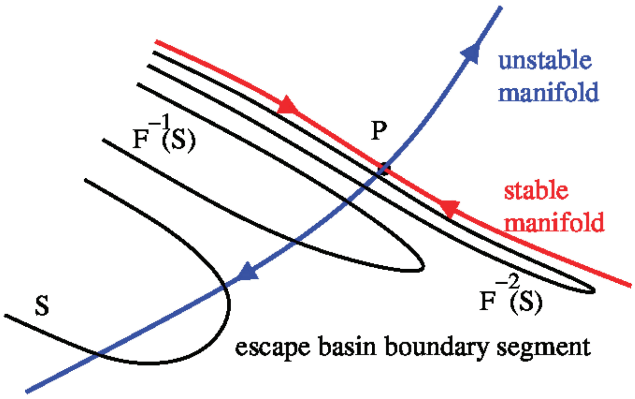

Figure 5. Schematic figure showing the accumulation of escape basin filaments at the stable manifold of a chaotic saddle.

the length of the lobes formed by the backward image increases to preserve areas [4].

Hence, if the segment S crosses the unstable (or stable) manifold of the chaotic saddle, the escape basin boundary is fractal. In the next section, we characterise quantitatively the fractal behaviour of the escape basin boundary using appropriate numerical diagnostics.

5. Uncertainty fraction and basin entropies

In this work we present two different quantitative characterisation of the escape basin boundary. The first is the computation of the box-counting dimension of the escape basin boundary by the uncertainty fraction method [25, 29] and the second is the determination of the so-called basin entropy and basin boundary entropy to quantify the degree of uncertainty due to the fractality of the escape basin boundary [23, 30]. The concept of uncertainty dimension has been long introduced in the literature of dissipative dynamical system for estimating the box-counting dimension of the basin boundary between two basins of attraction [25, 29]. It was also applied in open Hamiltonian (conservative) systems, for the boundary between escape basins [5].

We compute the uncertainty dimension of the escape basin boundary numerically by using the following method: we randomly pick up a large number of initial conditions b_0 in the interval $[b_m, b_{\rm esc}]$ for $\phi_0 = cte$, and for each one of them we iterate the map (32) and (33) a certain number of times, finding out its outcome and therefore to which basin the corresponding initial condition belongs.

For each initial condition (ϕ_0, b_0) we choose $(\phi_0, b_0 \pm \epsilon)$, where $\epsilon \ll 1$ is the uncertainty upto which the initial condition is known, and we again iterate the map until this perturbed initial condition escapes. Whenever the three points do not belong to the same escape basin, the condition b_0 is labelled as ϵ-uncertain initial condition. After a number ($N_0 = 10^3$) of initial conditions are tested the fraction $f(\epsilon)$ of ϵ-uncertain initial conditions is computed. These steps are repeated 10 times for each ϵ, which varied from 10^{-1} to about 10^{-10}. The fraction of uncertain initial conditions $f(\epsilon)$ is expected to increase with ϵ as a power-law $f(\epsilon) \sim \epsilon^{\alpha}$, where α is the so-called uncertainty exponent [25, 29].

The uncertainty dimension d quantifies the final-state uncertainty of the points belonging to basin boundary. Let d_p be the dimension of the phase space region to be considered, and let $N(\delta)$ be the minimum number of d_p-dimensional boxes of length δ necessary to cover the boundary. The box-counting dimension of the latter is

$$d = \lim_{\delta \to 0} \frac{\ln N(\delta)}{\ln(1/\delta)}, \tag{39}$$

such that $N(\delta)$ scales as δ^{-d} for small enough δ [3]. If we set $\delta = \epsilon$, the volume of the uncertain region in the phase space will be $N(\epsilon)$ times the volume of the d_p-dimensional cubes, which is ϵ^{d_p}. Since the initial conditions are uniformly chosen over the phase space region, the uncertain fraction is of the order of the total volume $N(\epsilon)\epsilon^{d_p} = \epsilon^{(d_p - d)}$. Thus, the uncertainty exponent results in $\alpha = d_p - d$. A rigorous analysis would show that the uncertainty dimension d coincides with the box-counting dimension of the escape basin boundary [29].

Since we set $\phi_0 = \text{const}$, we are considering a phase space cross section with $d_p = 1$, such that $\alpha = 1 - d$, in such a way that a smooth boundary with $d = 0$ has $\alpha = 1$, whereas $0 < \alpha < 1$ characterises a fractal basin boundary [25, 29]. We computed the uncertainty exponent for the escape basin boundary depicted in figures 3a–f for $\phi_0 = 0$ and $\phi_0 = \pi$. We have chosen these magnifications to cover chiefly fractal pieces of the boundary, and we obtained for the corresponding uncertainty dimensions for $\phi_0 = 0$ and $\phi_0 = \pi$ the values $d = 0.19 \pm 0.02$ and $d = 0.21 \pm 0.02$, respectively.

As the uncertainty exponent α is small, the fraction of ε-uncertain initial conditions is increasingly independent of the uncertainty ε itself. This means that the escape basin boundaries become so convoluted that virtually any attempt to decrease the fraction of uncertain conditions may be in vain.

An alternative measure of the unpredictability is to evaluate the area of each escape basin and the fraction it occupies of a given phase space area, whose ratio has been called basin stability by Menck *et al.* [31, 32]. It is understood that larger basins would be more stable, in the sense that small deviations of an initial condition would less probably result in uncertainty. Another approach to quantify the degree of final-state

uncertainty of a given basin is the computation of the so-called basin entropy [23, 30].

Let us consider the general case of N_A exiting in the phase space region Ω for an open system, and cover this region with a box grid of size ε. Each box contains an infinitely large number N of initial conditions, each of them leading to an escaping trajectory through a given exit labelled as $j = 1, 2, \ldots N_A$. We assign a probability p_{ij} that an initial condition in the ith box leads to an escape through the jth exit. Depending on the chosen box, the corresponding initial conditions may exit to a limited number of exits $m_i \leq N_A$. In the language of statistical mechanics m_i is the number of accessible microstates of the system [23].

Summing over the total number of microstates, the Gibbs entropy of the ith box is [30]

$$S_i = \sum_{j=1}^{m_i} p_{ij} \log\left(\frac{1}{p_{ij}}\right), \tag{40}$$

such that the entropy related to the whole grid is obtained by summing the contribution of each box $S = \sum_{i=1}^{N} S_i$. The basin entropy results by normalising this value $S_\mathrm{b} = S/N$. If we restrict the computation of the basin entropy only to the N_b boxes containing points of the boundary, we obtain the so-called boundary basin entropy $S_\mathrm{bb} = S/N_\mathrm{b}$.

In order to get an intuitive idea of the meaning of basin entropy let us consider two limiting situations: if we have a single exit ($N_A = 1$) the corresponding probability is equal to unity and hence $S_\mathrm{b} = 0$, i.e. no uncertainty at all. The opposite situation consists of completely randomised basins with N_A equiprobable escapes, for which $p_{ij} = 1/m_i$, which gives $S_\mathrm{b} = \log N_A$ as the upper bound of the basin entropy.

The basin boundary entropy S_bb measures the complexity of the basin boundary. Moreover, there is a threshold value of S_bb that separates basins with smooth boundaries from those with fractal boundaries. For example, suppose that our basins were separated by a smooth boundary. The number of boxes in the boundary will be negligible for the computation of the basin entropy in the boundary S_bb, since there are many more boxes with just one basin. Thus, the maximum possible value of S_bb that a smooth boundary can have is ln 2, which would be a pathological case where every box in the boundary contains equal proportions of two basins. Therefore, if $S_\mathrm{bb} > \ln 2$, the basin boundary is said to be fractal, but this is a sufficient but not necessary criterion for fractality, though, since some fractal basins do not fulfil this condition [10, 11, 30, 33].

We applied those concepts to the escape basins of figure 3, by computing the corresponding values of the basin entropy and basin boundary entropy. We varied the grid of phase space Ω considering 250×250, 200×200, 125×125 and 100×100 boxes, with 16, 25, 64, 100 initial conditions per box, respectively. For each grid point we computed a maximum number of 10^4 iterations of the map and exclude from the statistics those initial conditions leading to orbits that do not escape during this maximum iteration time.

Denoting by n_A, n_B and n_C the number of points escaping the system by asymptoting to the exits **A** (light ray falling on a black hole), **B** (light ray falling on the other black hole) and **C** (light ray going to infinity), respectively, the corresponding probabilities are given by

$$p_A = \frac{n_A}{n_A + n_B + n_C}, \qquad p_B = \frac{n_B}{n_A + n_B + n_C},$$
$$p_C = \frac{n_C}{n_A + n_B + n_C}, \tag{41}$$

and the entropy for each box is, from (40),

$$S = -p_A \log p_A - p_B \log p_B - p_C \log p_C. \tag{42}$$

The values of the basin entropy and basin boundary entropy of the region in figure 3 centred at $\phi_0 = 0$ are, respectively, $S_\mathrm{b} = (8.44 \pm 3.16) \times 10^{-5}$ and $S_\mathrm{bb} = 0.94 \pm 0.09$. For the region in figure 3 centred at $\phi_0 = \pi$ the corresponding values are $S_\mathrm{b} = (7.34 \pm 2.42) \times 10^{-5}$ and $S_\mathrm{bb} = 0.93 \pm 0.08$. For the two cases of ϕ_0 the value of basin entropy S_b is low, thanks to the fact that most boxes considered in this region contains initial conditions that escape through a single exit. The statistics become relatively poor and the dispersions are relatively large. However, the entropy of the boundary of basin S_bb obeys the inequality $S_\mathrm{bb} > \ln 2$, i.e. the basin boundary is indeed fractal, as the uncertainty dimension has already pointed out.

6. Wada escape basin boundaries

If, for two basins the boundary is a fractal curve, one may ask what this would mean for three or more exit basins. The answer lies in the so-called Wada property: if the boundary between two basins is smooth, three of such basins have only one common boundary point. However, if the boundary is fractal there may be an infinite number of such common points [34].

Let B be an escape basin. It has a boundary point P if every open neighbourhood of P intersects the basin B and at least another basin. The set of all boundary points of that basin is defined as the corresponding basin boundary. The boundary point P is called a Wada point if every open neighbourhood of P intersects at least three different basins [35]. A basin boundary is said to possess the Wada property if every boundary point of B is a Wada point, such that the boundary of such a basin is a Wada escape basin boundary. A necessary (but not

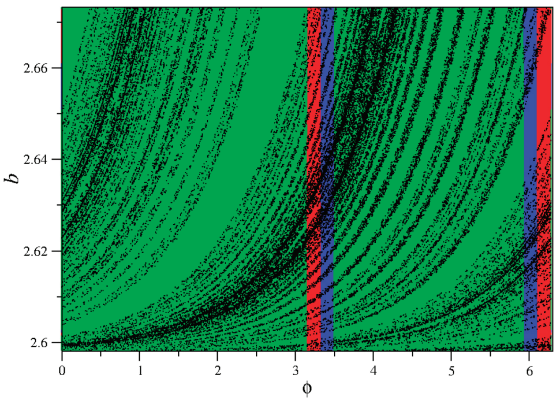

Figure 6. Escape basins of the scattering map for $D = 15$. The colour code for the basins is the same as in figure 2. The black curve is a segment of the unstable manifold of a periodic orbit embedded in the chaotic region.

sufficient) condition for the Wada property to exist is that the unstable manifold of an unstable periodic orbit P belonging to this boundary must intersect every escape basin [36, 37].

The Wada boundaries have important physical consequences, since in this case any boundary point turns to be arbitrarily close to points of all escape basins [38]. Hence it is not possible to say with certainty to which basin will the trajectory asymptote to, even if we could improve the uncertainty. This is a case of extreme final-state sensitivity.

In order check the validity of condition for the Wada property in our system, in figure 6 we plot (in black) a segment of the unstable manifold of some periodic orbit embedded in the chaotic region together with the escape basin. It is clearly seen that such manifold intercepts points of the blue, red and green basins. The successive magnifications of the escape basin, previously plotted in figure 3 show that stripes of all basins coexist in increasingly finer scales, suggesting that at least some of the boundary points have the Wada property. Thus, if any but not all boundary points do, then we have only partial fulfilment of this property.

7. Conclusions

The scattering of light rays by a binary black hole system is an outstanding example of open Hamiltonian systems. Being a non-integrable Hamiltonian system, one expects the presence of many dynamical features, like invariant tori, periodic islands, homoclinic points and chaotic motion. On the other hand, being an open system the chaotic motion is typically transient, since the fate of an incident light ray is either to escape to infinity or fall into one of the black holes. In these cases, one is interested to obtain the respective exit basin, or the set of initial conditions leading to a given outcome. In non-integrable open Hamiltonian systems, the exit basins and their common boundary are fractal structures, chiefly due to the presence of a non-attractive invariant set called chaotic saddle.

In this paper we considered the light ray scattering by a binary black hole system from the point of view of an open Hamiltonian systems, focusing on the fractal structures present in the chaotic dynamics. The equations of general relativity for a light ray in the gravitational field of a binary Schwarzschild black hole system were integrated approximately to obtain a discrete-time map, which exhibits chaotic dynamics for a wide range of its parameters (the most important being the distance between black holes). The chaotic dynamics here is transient, though, for the light rays can either escape to infinity or fall into one of the black holes.

The fractal exit basin boundaries for this systems were investigated by computing the so called uncertainty exponent, which yields a numerical estimate of the fractal dimension of the exit basin boundary. Moreover, the chaotic saddle responsible for the latter has been evidenced numerically. In most of the cases analysed the escape basin boundary dimension has been found to be about 0.20. Another quantitative characterisation of the fractal exit basin boundaries is the basin entropy, which measures the uncertainty of the final-state when more than one outcome exists for a typical trajectory.

The basin entropy, which is basically the information entropy related to the probability of going to a given basin, has been found to vary according to the magnification used to represent the exit basins. The basin boundary entropy, however, which takes into account only the intervals containing basin boundary points, shows consistently uniform values, compatible with the basin boundary dimension of 0.20 obtained through a different method.

Finally, in the present paper we described the Wada property, which is typical for systems with three or more basins with a fractal basin boundary. The Wada property means that every boundary point is such that an arbitrarily small neighbourhood centred at that point contains points of the three (or more) basins. It is actually an extreme form of final-state uncertainty. We have verified the presence of the Wada property by showing that the unstable manifold of some periodic orbit embedded in the chaotic saddle intercepts all three basins. If this intersection occurs once, it will occur an infinite number of times.

In summary, we have studied some fractal structures present in the chaotic motion of a light ray under the gravitational field of two Schwarzschild black holes, a problem which is classically non-integrable and

has a non-attractive chaotic invariant set responsible for chaotic transient dynamics. Such fractal structures are responsible for various signatures of the so-called chaotic scattering, which is a phenomenon ubiquitous in non-integrable open Hamiltonian systems. Further investigation in the footsteps of the present paper will take into account black holes with charge, for which the Reissner–Nordström metric must be used instead. The general procedure outlined in this paper, which is an approximate solution of the equations of motion, can be used to take into account this metric with charge effects.

The strong lensing effect caused by the black holes' gravitational field generate an infinite number of images of the light source. These images are directly related to the regions whereby the photon escapes out to infinity. From our results concerning the escape basins of the open Hamiltonian system represented by the scattering map, we see that the escape regions have a larger area than those regions for which the photon is captured by the black holes. Moreover we consider the effects of each black hole individually, without taking into account the influence of the other black hole. Hence we do not expect any drastic changes in the analysis of the images due to the lensing effect in the case of two black holes investigated in this paper.

Acknowledgements

The authors acknowledge useful suggestions by Prof. G. M. Kremer (Curitiba) and the valuable help of Mr Eduardo L. Brugnago. This work was supported by grants from the Brazilian Government Agencies CAPES, CNPq (Proc. 301019/2019-3) and São Paulo Research Foundation (FAPESP, Brazil), under Grant No. 2018/03211-6.

References

[1] S Weinberg, *Gravitation and Cosmology: Principles and Applications of the General Theory of Relativity* (Wiley, New York, 1972)
[2] C P Dettmann, N E Frankel and N J Cornish, *Fractals* **3**, 161 (1995)
[3] J Aguirre, R L Viana and M A F Sanjuán, *Rev. Mod. Phys.* **81**, 333 (2009)
[4] A Péntek, Z Toroczkai, T Tél, C Grebogi and J A Yorke, *Phys. Rev. E: Stat. Phys., Plasmas, Fluids, Relat. Interdiscip. Top.* **51**, 4076 (1995)
[5] S Bleher, C Grebogi, E Ott and R Brown, *Phys. Rev. A* **38**, 930 (1988)
[6] J Aguirre, J C Vallejo and M A F Sanjuán, *Phys. Rev. E: Stat., Nonlinear, Soft Matter Phys.* **64**, 066208 (2001)
[7] R Barrio, F Blesa and S Serrano, *Europhys. Lett.* **82**, 10003 (2008)
[8] E G Altmann, J C Leitão and J V Lopes, *Chaos* **22**, 026114 (2012)
[9] M Hansen, D da Costa, I L Caldas and E D Leonel, *Chaos Solitons Fractals* **106**, 355 (2018)
[10] A C Mathias, R L Viana, T Kroetz and I L Caldas, *Phys. A* **469**, 681 (2017)
[11] A C Mathias, T Kroetz, I L Caldas and R L Viana, *Chaos Solitons Fractals* **104**, 588 (2017)
[12] C Misner, K S Thorne and J A Wheeler, *Gravitation* (W H Freeman, New York, 1973)
[13] B P Abbot *et al.*, *Phys. Rev. Lett.* **116**, 061102 (2016)
[14] A Daza, J O Shipley, S R Dolan and M A F Sanjuán, *Phys. Rev. D* **98**, 084050 (2018)
[15] S D Majumdar, *Phys. Rev.* **72**, 390 (1947)
[16] A Papapetrou, *Proc. R. Ir. Acad., Sect. A* **51**, 191 (1947)
[17] G Contopoulos, *Astron. Astrophys.* **231**, 41 (1990)
[18] G Contopoulos, H E Kandrup and D Kauffman, *Phys. D* **64**, 310 (1993)
[19] P V P Cunha and C A R Herdeiro, *Gen. Relat. Gravit.* **50**, 42 (2018)
[20] A P S de Moura and P S Letelier, *Phys. Rev. E: Stat. Phys., Plasmas, Fluids, Relat. Interdiscip. Top.* **62**, 4784 (2000)
[21] S Chandrasekhar, *The Mathematical Theory of Black Holes* (Oxford University Press, Oxford, 1998)
[22] V Bozza, *Phys. Rev. D* **66**, 103001 (2002)
[23] A Daza, A Wagemakers, B Georgeot, D Guéery-Odelin and M A F Sanjuán, *Sci. Rep.* **6**, 31416 (2016)
[24] S L Shapiro and S A Teulkosky, *Black Holes, White Dwarfs and Neutron Stars: The Physics of Compact Objects* (Wiley, New York, 1983)
[25] S W McDonald, C Grebogi, E Ott and J A Yorke, *Phys. D* **17**, 125 (1985)
[26] G-H Hsu, E Ott and C Grebogi, *Phys. Lett. A* **127**, 199 (1988)
[27] E G Altmann, J S E Portela and T Tél, *Rev. Mod. Phys.* **85**, 869 (2013)
[28] L Poon, J Campos, E Ott and C Grebogi, *Int. J. Bifurcation Chaos* **6**, 251 (1996)
[29] C Grebogi, S W McDonald, E Ott and J A Yorke, *Phys. Lett. A* **99**, 415 (1983)
[30] A Daza, B Georgeot, D Guéry-Odelin, A Wagemakers and M A F Sanjuán, *Phys. Rev. A* **95**, 013629 (2017)
[31] P J Menck, J Heitzig, N Marwan and J Kurths, *Nat. Phys.* **9**, 89 (2013)
[32] P Menck, J Heitzig, J Kurths and H J Schellnhuber, *Nat. Commun.* **5**, 3969 (2014)
[33] M Mugnaine, A C Mathias, M S Santos, A M Batista, J D Szezech Jr and R L Viana, *Phys. Rev. E* **97**, 012214 (2018)
[34] J Kennedy and J A Yorke, *Phys. D* **51**, 213 (1991)
[35] H E Nusse and J A Yorke, *Science* **271**, 1376 (1996)
[36] H E Nusse and J A Yorke, *Phys. D* **90**, 242 (1996)
[37] Z Toroczkai, G Károlyi, A Péntek, T Tél, C Grebogi and J A Yorke, *Phys. A* **239**, 235 (1997)
[38] J Kennedy and J A Yorke, *Phys. D* **51**, 213 (1991)